AIAA JOURNAL
Vol. 41, No. 10, October 2003

# Analysis of Subgrid-Scale Torque for Large-Eddy Simulation of Turbulence

J. S. Marshall* and M. L. Beninati†
*University of Iowa, Iowa City, Iowa 52242*

**A study is performed of the vorticity source induced by filtering the nonlinear terms of the Navier–Stokes equation, as used in large-eddy simulation of turbulent flows. In analogy to the subgrid-scale (SGS) stress, this vorticity source is referred to as the subgrid-scale torque. The SGS torque results from derivatives of the part of the SGS stress and force terms that play a role in modifying the filtered velocity field. Other parts of the SGS stress and force modify pressure but have no influence on velocity field in a constant-density flow and are, therefore, not dynamically significant. The total dissipation rate due to the SGS flow is shown to depend only on the part of the SGS force induced by the SGS torque. With a series of examples with increasing complexity, it is shown that the SGS stress and force are often dominated by terms that generate no SGS torque. With use of the scale-similarity model, both for isotropic turbulence and for turbulence near a large-scale vortex structure, it is demonstrated that LES closure models can sometimes yield reasonably good results in a priori tests for prediction of SGS stress and force, while yielding poor predictions for SGS torque. This conclusion is consistent with the common observation that the scale-similarity model yields good results in a priori tests (when only the SGS stress is examined) but nevertheless has insufficient dissipation in a posteriori tests.**

## Nomenclature

| | | |
|---|---|---|
| $A$ | = | forcing amplitude for direct numerical simulation |
| $a$ | = | initial vortex core radius |
| $\boldsymbol{b}$ | = | vector potential of the subgrid-scale force $\boldsymbol{g}$ |
| $C_{AB}$ | = | correlation between two quantities $A$ and $B$ |
| $C_S$ | = | Smagorinsky constant |
| $c$ | = | vortex axial stretching rate |
| $D$ | = | local dissipation rate |
| $\boldsymbol{D}$ | = | deviatoric part of the subgrid-scale stress tensor |
| $E$ | = | enstrophy production rate |
| $\boldsymbol{e}_r, \boldsymbol{e}_\phi, \boldsymbol{e}_z$ | = | base vectors in the $r$, $\phi$, and $z$ directions of a cylindrical polar coordinate system |
| $\boldsymbol{f}$ | = | forcing vector used in numerical simulation of isotropic turbulence |
| $G_\Delta$ | = | filter function with length scale $\Delta$ |
| $\boldsymbol{g}$ | = | subgrid-scale force |
| $\boldsymbol{h}$ | = | vector defined by equation preceding Eq. (11) |
| $k$ | = | wave number |
| $k_c$ | = | cutoff wave number |
| $\boldsymbol{L}$ | = | tensor defined by the Germano identity [Eq. (9)] |
| $\ell$ | = | integral length scale |
| $\boldsymbol{n}$ | = | unit normal of a closed surface $S$ |
| $\boldsymbol{P}$ | = | projection tensor for the spectral solution of the Navier–Stokes equations |
| $\boldsymbol{R}$ | = | skew-symmetric tensor whose axial vector is $\boldsymbol{g}$ |
| $Re_V$ | = | vortex Reynolds number |
| $Re_\lambda$ | = | microscale Reynolds number of the turbulence |
| $\boldsymbol{S}$ | = | rate of deformation tensor |
| $\boldsymbol{s}$ | = | subgrid-scale torque |
| $\boldsymbol{T}$ | = | subgrid-scale stress tensor |
| $t$ | = | time |
| $\boldsymbol{u}$ | = | velocity vector with components $u$, $v$, and $w$ in the $r$, $\phi$, and $z$ directions |
| $u'$ | = | root-mean-square velocity magnitude |
| $\boldsymbol{x}$ | = | position vector |
| $\boldsymbol{Y}$ | = | tensor defined by Eq. (8) |
| $\beta$ | = | ratio of the turbulence initial root-mean square velocity to the maximum azimuthal velocity of the vortex |
| $\Gamma$ | = | vortex circulation |
| $\Delta_i$ | = | filter length scale in $i$ direction |
| $\delta_{ij}$ | = | Kronecker delta |
| $\varepsilon$ | = | average dissipation rate |
| $\varepsilon_{ijk}$ | = | permutation symbol |
| $\eta$ | = | Kolmogorov length scale of the turbulence |
| $\lambda$ | = | Taylor microscale of the turbulence |
| $\nu$ | = | kinematic viscosity |
| $\nu_T$ | = | eddy viscosity |
| $\rho$ | = | density |
| $\sigma$ | = | vortex core radius |
| $\phi$ | = | scalar potential of subgrid-scale force $\boldsymbol{g}$ |
| $\boldsymbol{\omega}$ | = | vorticity vector |

*Superscripts*

| | | |
|---|---|---|
| $\bar{f}$ | = | convolution filter of a function $f(\boldsymbol{x}, t)$ with small filter length scale $\bar{\Delta}$ |
| $\tilde{f}$ | = | convolution filter of a function $f(\boldsymbol{x}, t)$ with large filter length scale $\tilde{\Delta}$ |

## I. Introduction

LARGE-EDDY simulation (LES) attempts to follow the large scales of turbulent flows computationally without directly solving for motion at the small scales by solving a filtered form of the Navier–Stokes equations. Filtering of the nonlinear convective acceleration term gives rise to an additional force having the form of the divergence of the subgrid-scale (SGS) stress $T_{ij} \equiv -(\overline{u_i u_j} - \overline{u_i}\,\overline{u_j})$, where $\boldsymbol{u}$ is the velocity vector and an overbar denotes a filtering process. However, as pointed out by Meneveau and Katz,[1] some parts of the SGS force can be expressed as the gradient of a scalar, and hence in a constant-density flow, these terms modify the pressure field without affecting the velocity field. The parts of the SGS force that are dynamically significant, that is, which do affect the velocity field, possess a nonzero curl, giving rise to a nonzero source of vorticity (or SGS torque).

Received 18 October 2001; revision received 8 October 2002; accepted for publication 1 May 2003. 

*Professor, Department of Mechanical and Industrial Engineering and IIHR-Hydroscience and Engineering; jeffrey-marshall@uiowa.edu.

†Graduate Assistant, Department of Mechanical and Industrial Engineering and IIHR-Hydroscience and Engineering.

Several investigators have studied the relationship between the SGS stress and different aspects of the flow structure. For instance, Domaradzki et al.[2] examine decaying turbulence within a Taylor–Green vortex at microscale Reynolds number decreasing from 1000 to 70. They observe large regions of both forward and backward energy transfer, both of which are important for the dynamics of the large scales of motion. The motion of the resolved scales in the vicinity of a cutoff wave number $k_c$ is found to depend significantly only on modes with wave number less than $2k_c$, with higher wave number modes having negligible effect.

Kerr et al.[3] examine the relationship between turbulent vorticity structures and various aspects of the SGS energy transport and dissipation based on analysis of direct numerical simulation (DNS) data for isotropic turbulence with Reynolds numbers of 64 and 258. This study makes three conclusions of interest in the present investigation: 1) subgrid energy transfer coincides with boundaries of regions of strong enstrophy production, 2) energy backscatter coincides with regions of large correlation of resolved vorticity and subgrid velocity, and 3) energy forwardscatter is dominated by the correlation of subgrid vorticity and resolved velocity.

Meneveau and Katz[1] use conditional averaging to associate the SGS force with different flow features, such as strain rate, vorticity, and energy dissipation rate, based on experimental data from constant-density flow in a turbulent jet and in turbulence undergoing rapid axisymmetric expansion. In the approximately locally isotropic turbulence from the jet flow, they observe high correlation between SGS force magnitude and both strain rate and dissipation rate. However, in these regions the SGS force vectors are oriented in the radial direction (relative to some central point) and exhibit azimuthal symmetry, rather like the velocity field emanating from a source or a sink. Because the SGS force in these regions is purely radial, it can be expressed as the gradient of a scalar and is, hence, not dynamically significant. In the case of rapidly strained turbulence undergoing axisymmetric expansion, SGS force opposing the mean deformation is observed in regions of strong positive dissipation, and SGS force enhancing the mean deformation is observed in regions of strong negative SGS dissipation. Meneveau and Katz[1] further note that the predictions of the scale-similarity model[4] generally have higher SGS force magnitude and extend over larger distances than the exact data.

The objective of the present paper is to examine the relationship between the SGS torque and other quantities characterizing the turbulence and to demonstrate the importance of accurate prediction of SGS torque in a priori tests of LES closure models. A review of theoretical aspects of the filtered Navier–Stokes and vorticity transport equations and a brief summary of common SGS modeling approaches is given in Sec. II. After removing the dynamically insignificant part of the SGS stress, it is observed that (in a constant-density flow) the SGS force is nonzero only in flow regions with nonvanishing vorticity. We also show that the total energy dissipation rate can be expressed as an integral over the part of the SGS force induced by the SGS torque, such that the part of the SGS force that can be written as a gradient of a scalar affects the local dissipation rate but has no effect on the overall dissipation rate. In Sec III, the SGS torque in two simple vortex flows is examined, which might be regarded as building blocks for more complex flows. SGS torque in forced isotropic turbulence is examined in Sec. IV and that in decaying turbulence surrounding a large-scale vortex is examined in Sec. V. This latter flow is representative of the interaction between large-scale coherent vortices and smaller-scale turbulence in high-Reynolds-number turbulent flows. In Secs. IV and V, exact DNS data for SGS force and torque are compared with predictions of the scale-similarity model,[4] which has been found by previous investigators to yield predictions with high correlation to exact data. Conclusions are presented in Sec. VI.

## II. Theory

### A. SGS Torque

LES methods are based on numerically evolving a filtered form of the Navier–Stokes equations. If the filtering is performed in physical space, it is typically of the convolution type, such that for some function $f(\boldsymbol{x}, t)$ we write

$$\bar{f}(\boldsymbol{x}, t) = \int_V G_{\Delta_i}(x_i - x_i') f(\boldsymbol{x}', t)\, \mathrm{d}v' \tag{1}$$

where $G_{\Delta_i}(x_i - x_i')$ is a homogeneous filter function that decays with length scale $\Delta_i$ in the $i$ direction, $V$ is the entire space occupied by the fluid, and an overbar denotes a filtered variable. Because a homogeneous filtering operation commutes with temporal and spatial differentiation, the filtered continuity and Navier–Stokes equations for an incompressible fluid with uniform density are

$$\nabla \cdot \bar{\boldsymbol{u}} = 0 \tag{2a}$$

$$\frac{\partial \bar{\boldsymbol{u}}}{\partial t} + (\bar{\boldsymbol{u}} \cdot \nabla)\bar{\boldsymbol{u}} = -\frac{1}{\rho}\nabla \bar{p} + \nabla \cdot [2\nu \bar{\boldsymbol{S}} + \boldsymbol{T}] \tag{2b}$$

where $\bar{\boldsymbol{S}} = (\frac{1}{2})[\nabla \bar{\boldsymbol{u}} + (\nabla \bar{\boldsymbol{u}})^T]$ is the filtered rate of deformation tensor and the components of the SGS stress tensor are

$$T_{ij} \equiv -(\overline{u_i u_j} - \overline{u_i}\,\overline{u_j}) \tag{3}$$

The filtering operation can also be performed for the vorticity–velocity form of the Navier–Stokes equations. The filtered vorticity $\bar{\boldsymbol{\omega}} = \nabla \times \bar{\boldsymbol{u}}$ in a constant-density flow is governed by the transport equation

$$\frac{\partial \bar{\boldsymbol{\omega}}}{\partial t} + (\bar{\boldsymbol{u}} \cdot \nabla)\bar{\boldsymbol{\omega}} = (\bar{\boldsymbol{\omega}} \cdot \nabla)\bar{\boldsymbol{u}} + \nu \nabla^2 \bar{\boldsymbol{\omega}} + \nabla \times \boldsymbol{g} \tag{4}$$

where the SGS force $\boldsymbol{g}$ has components

$$g_i \equiv -\varepsilon_{ijk}(\overline{\omega_j u_k} - \overline{\omega_j}\,\overline{u_k}) \tag{5}$$

We refer to $\boldsymbol{s} \equiv \nabla \times \boldsymbol{g}$ as the SGS torque. It is clear from its definition that $\boldsymbol{g}$ vanishes in any irrotational flow region. The vector $\boldsymbol{g}$ is the axial vector of a skew-symmetric tensor $\boldsymbol{R}$, defined by

$$R_{ij} \equiv \varepsilon_{ijk} g_k = -(\overline{\omega_i u_j} - \overline{\omega_i}\,\overline{u_j}) + (\overline{\omega_j u_i} - \overline{\omega_j}\,\overline{u_i}) \tag{6}$$

The SGS force and torque can be written as $\boldsymbol{g} = \nabla \cdot \boldsymbol{D}$ and $\boldsymbol{s} = \nabla \cdot \boldsymbol{R}$, respectively, where $D_{ij} \equiv T_{ij} - (\frac{1}{3})T_{kk}\delta_{ij}$ is the deviatoric part of the SGS stress $\boldsymbol{T}$. Thus, the tensor $\boldsymbol{R}$ plays a similar role in the vorticity transport equation as the deviatoric part of $\boldsymbol{T}$ plays in the momentum equation. The isotropic part of $\boldsymbol{T}$ can be incorporated into the pressure gradient term and, hence, has no influence on the filtered velocity $\bar{\boldsymbol{u}}$. Moreover, using the Helmholtz decomposition to write $\boldsymbol{g}$ as the sum of irrotational and rotational parts, where the irrotational part can be combined with the pressure gradient, we see that the only dynamically significant part of the SGS force is that which yields a nonzero SGS torque.

The eddy–viscosity (Smagorinski) model approximates the deviatoric part of the SGS stress tensor as

$$D_{ij} \cong 2\nu_T \bar{S}_{ij}, \qquad \nu_T = C_S^2 \Delta^2 |\bar{\boldsymbol{S}}| \tag{7}$$

where $\nu_T$ is the eddy viscosity and $|\bar{\boldsymbol{S}}| \equiv (2\bar{S}_{ij}\bar{S}_{ij})^{1/2}$ is the modulus of $\bar{\boldsymbol{S}}$. A typical value for the constant $C_S$ is about 0.15 (Ref. 5).

The scale-similarity model[4] uses two filters, with length scales $\bar{\Delta}$ and $\tilde{\Delta}$. Applying these filters in series, we define a tensor $\boldsymbol{Y}$ by

$$Y_{ij} \equiv -(\widetilde{\overline{u_i u_j}} - \widetilde{\overline{u_i}}\,\widetilde{\overline{u_j}}) \tag{8}$$

The Germano identity (Ref. 6) gives

$$L_{ij} \equiv Y_{ij} - \tilde{T}_{ij} = -(\widetilde{\overline{u_i u_j}} - \widetilde{\overline{u_i}}\,\widetilde{\overline{u_j}}) \tag{9}$$

where the right-hand side can be determined by a second filtering of the filtered velocity field $\bar{\boldsymbol{u}}$. The scale-similarity model assumes that the SGS stress can be approximated by the difference term in Eq. (9). Thus, if the filter with length scale $\bar{\Delta}$ is associated with the

minimum computational resolution, the second filter with a larger length scale $\tilde{\Delta} > \bar{\Delta}$ is used to estimate the SGS stress as

$$T_{ij} \cong -(\widetilde{\overline{u_i}\,\overline{u_j}} - \widetilde{\overline{u_i}}\,\widetilde{\overline{u_j}}) \tag{10}$$

The scale-similarity procedure can also be used to develop an expression directly for the SGS force $\boldsymbol{g}$. In particular, if a vector $\boldsymbol{h}$ is defined by sequential application of the two filters as $h_i \equiv -\varepsilon_{ijk}(\widetilde{\overline{\omega_j}\,\overline{u_k}} - \widetilde{\overline{\omega_j}}\,\widetilde{\overline{u_k}})$, an identity similar to the Germano identity (9) can be written for the difference between $\boldsymbol{h}$ and the filtered value $\tilde{\boldsymbol{g}}$ of $\boldsymbol{g}$ as

$$h_i - \tilde{g}_i = -\varepsilon_{ijk}(\widetilde{\overline{\omega_j}\,\overline{u_k}} - \widetilde{\overline{\omega_j}}\,\widetilde{\overline{u_k}}) \tag{11}$$

The identity (11) was used by Mansfield et al.[7] to obtain the coefficients for a dynamic Smagorinsky-type model for $\boldsymbol{g}$, which was then implemented in a vortex particle method for turbulent flows. Alternatively, in the context of a scale-similarity model, one would approximate the SGS force $\boldsymbol{g}$ by the right-hand side of Eq. (11).

### B. Relationship of SGS Torque to Dissipation Rate

The local dissipation rate $D$ due to the SGS stress can be expressed in an incompressible flow as the scalar product of the deviatoric part $\boldsymbol{D}$ of the SGS stress with the velocity gradient, or using chain rule,

$$D = D_{ij}\frac{\partial u_i}{\partial x_j} = \frac{\partial}{\partial x_j}(D_{ij}u_i) - u_i\frac{\partial D_{ij}}{\partial x_j} \tag{12}$$

The last term in Eq. (12) is simply the inner product of the velocity and the SGS force vector $\boldsymbol{g}$. Applying the Helmholtz decomposition to $\boldsymbol{g}$, we can write

$$\boldsymbol{g} = \nabla\phi + \nabla \times \boldsymbol{b} \tag{13}$$

where $\boldsymbol{b}$ is a solenoidal vector field. Taking the curl of Eq. (13) gives $\boldsymbol{s} = -\nabla^2\boldsymbol{b}$, the particular solution of which yields the vector $\boldsymbol{b}$ as an integral over the SGS torque as

$$\boldsymbol{b}(\boldsymbol{x}, t) = \frac{1}{4\pi}\int_V \frac{\boldsymbol{s}(\boldsymbol{x}', t)}{|\boldsymbol{x} - \boldsymbol{x}'|}\,\mathrm{d}v'$$

$$\hat{\boldsymbol{g}}(\boldsymbol{x}, t) \equiv \nabla \times \boldsymbol{b} = \frac{1}{4\pi}\int_V \frac{\boldsymbol{s}(\boldsymbol{x}', t) \times (\boldsymbol{x} - \boldsymbol{x}')}{|\boldsymbol{x} - \boldsymbol{x}'|^3}\,\mathrm{d}v' \tag{14}$$

where $V$ is the entire volume occupied by the flow and $\hat{\boldsymbol{g}}$ is the part of the SGS force induced by the SGS torque.

Integrating the local dissipation rate over the flow volume $V$ yields the total dissipation rate as

$$\int_V D\,\mathrm{d}v = \int_S (\boldsymbol{u}\cdot\boldsymbol{D}\cdot\boldsymbol{n} - \phi\boldsymbol{u}\cdot\boldsymbol{n})\,\mathrm{d}a - \int_V \boldsymbol{u}\cdot\hat{\boldsymbol{g}}\,\mathrm{d}v \tag{15}$$

where $S$ is the boundary of $V$. Applying the no-slip condition on the fixed surface $S$ (or letting $S$ move out to infinity in an unbounded flow), the surface integral in Eq. (15) vanishes. Integrating by parts for the volumetric integral in Eq. (15), we can alternatively write the total dissipation rate as an integral over the product of the vorticity vector and the vector potential $\boldsymbol{b}$ of the SGS force as

$$\int_V D\,\mathrm{d}v = \int_V \boldsymbol{\omega}\cdot\boldsymbol{b}\,\mathrm{d}v \tag{16}$$

Thus, we conclude that the part of the SGS force that can be written as the gradient of a scalar [this first term on the right-hand side of Eq. (13)] makes no contribution to the total energy dissipation rate of the flow.

## III. Simple Examples

We have observed in Sec. II that the dynamically significant part of the SGS force occurs in regions with nonzero vorticity. In an attempt to develop physical intuition for the SGS torque, we examine in the current section the exact SGS force and torque fields produced by two simple axisymmetric flows. Because the SGS force (5) is Galilean invariant, the addition of a uniform translation velocity does not alter these axisymmetric results.

The most elementary axisymmetric vortex flow is a columnar vortex, an example of which is the Lamb vortex with velocity field $\boldsymbol{u} = v(r)\boldsymbol{e}_\phi = (\Gamma/2\pi r)[1 - \exp[-(r/\sigma)^2]\boldsymbol{e}_\phi$. The exact SGS force $\boldsymbol{g}$ is oriented in the radial direction and has a form $\boldsymbol{g} = g(r)\boldsymbol{e}_r$. Because the SGS force can be rewritten as the gradient of a function,

$$f(r) \equiv \int_0^r g(\xi)\,\mathrm{d}\xi$$

it can be combined with the pressure gradient term in the filtered Navier–Stokes equations and, thus, has no effect on the velocity field. Associated with this observation, the exact SGS torque vanishes for this flow.

The result of vanishing exact SGS torque for a columnar vortex is unaffected by addition of an axial flow $w(r)$ within the vortex core. To find an axisymmetric flow with nonvanishing SGS torque, we must look to cases with nonzero radial velocity or variation of the flowfield in the axial direction. The simplest such case is Burger's vortex, involving a columnar vortex that is stretched along its axis, for which the velocity field at a given instant of time is $\boldsymbol{u} = -cr\boldsymbol{e}_r + v(r)\boldsymbol{e}_\phi + 2cz\boldsymbol{e}_z$. The azimuthal velocity profile $v(r)$ is the same as given earlier for the Lamb vortex. The constant $c$ denotes the axial stretching rate nondimensionalized by the vortex circulation over the core radius squared. Burger's vortex exhibits nonzero SGS torque of the form $\boldsymbol{s} = s(r)\boldsymbol{e}_z$, where $s = (1/r)\partial(rg_\phi)/\partial r$. The azimuthal component of the SGS force is related to the product of the radial velocity and the axial vorticity by $g_\phi = -(\overline{\omega_z u_r} - \overline{\omega_z}\,\overline{u_r})$, such that the dimensionless product $s\sigma^2/c\Gamma$ is a function only of $r/\sigma$ for a given filter size. Figure 1 shows a plot of the dimensionless SGS torque for a Burger's vortex with different filter lengths. This result was obtained using a discrete Gaussian filter, which is radially weighted to mimic an isotropic three-dimensional filter. The SGS torque acts to decrease the axial vorticity within the center of the vortex core and to increase the axial vorticity along the periphery of the vortex core. Because the integral of the SGS torque over the vortex cross section vanishes, it has no effect on the net vortex circulation. The maximum value of the SGS torque magnitude occurs on the vortex centerline and is observed to increase substantially with increase in filter size.

It is of interest that the eddy–viscosity (Smagorinsky) model for the SGS stress yields the incorrect result of azimuthally oriented

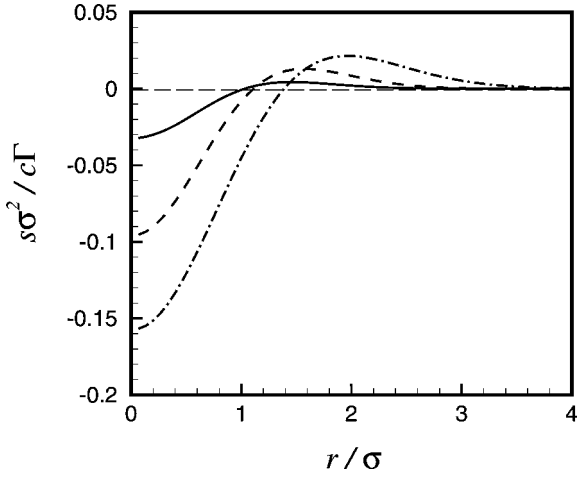


**Fig. 1 Axial SGS torque for a Burger's vortex with filter sizes ——, $\Delta/\sigma = 0.24$; – – –, $\Delta/\sigma = 0.48$; and –·–·–, $\Delta/\sigma = 0.96$.**

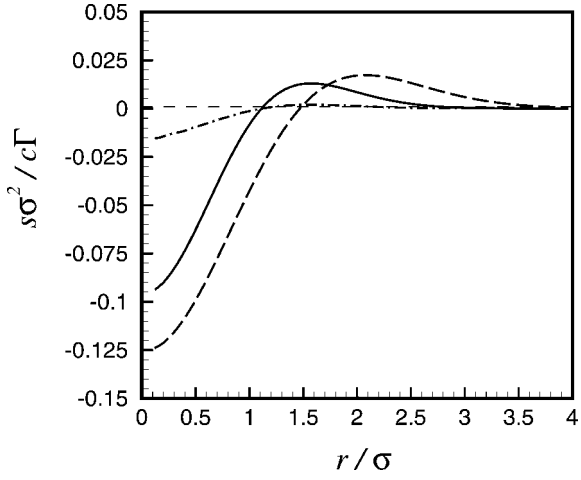


**Fig. 2 Comparison of computed SGS vorticity source for a Burger's vortex with filter size $\Delta/\sigma = 0.48$ for ——, exact data; – – –, prediction of scale-similarity model; and –·–·–, the Smagorinski model with $C_S = 0.15$.**

SGS force and nonvanishing SGS torque for the Lamb vortex, and yet it produces a radial spreading of the vorticity that is qualitatively similar to that produced by the exact SGS torque for the Burgers vortex. The scale-similarity model by construction satisfies the requirement of radial SGS force and zero SGS torque for the Lamb vortex and has a similar vorticity spreading effect for the Burgers vortex. A plot showing a comparison between the exact SGS torque and the predictions of the eddy-viscosity and scale-similarity models is given in Fig. 2 for a case with filter length $\Delta = 0.48$. The minimum value of $s_z$ in the exact data is about $-0.1$. The minimum value of $s_z$ in the Smagorinski model ($-0.02$) has far too small magnitude, although this could presumably be modified by adjustment of the Smagorinsky constant $C_S$. The minimum $s_z$ value predicted by the scale-similarity model ($-0.125$) has somewhat greater magnitude than the exact data, which is consistent with the observation that the value of $s_z$ in the vortex core becomes more negative as the filter size increases.

Turbulence properties for other simple vortex models have been investigated by several investigators. For instance, turbulence properties of the Burgers vortex are examined by Townsend,[8] and turbulence properties of the Lundgren stretched spiral vortex[9] are reported by Pullin et al.,[10] Saffman and Pullin,[11,12] and Pullin and Saffman,[13] leading to the vortex-based SGS stress model of Misra and Pullin.[14] These authors, however, do not consider the SGS torque.

## IV. Isotropic Turbulence

Direct numerical computations of forced isotropic turbulence are performed using a code similar to that of Vincent and Meneguzzi,[15] which employs a pseudospectral method with second-order Adams–Bashforth time stepping and exact integration of the viscous term. Results with and without dealiasing are found to exhibit no significant differences at the large scales, and so dealiasing is not used in the current computations to consider the broadest possible spectral range. The spectral Navier–Stokes equations are evolved in time after having been projected onto a divergence-free space using the operator $P_{ij} = k_i k_j/k^2 - \delta_{ij}$ according to

$$\hat{\boldsymbol{u}}^{n+1} = \hat{\boldsymbol{u}}^n \exp(-\nu k^2 \Delta t) + \Delta t \boldsymbol{P} \cdot \left[\tfrac{3}{2}(\boldsymbol{u}\times\boldsymbol{\omega})^n \exp(-\nu k^2 \Delta t) - \tfrac{1}{2}(\boldsymbol{u}\times\boldsymbol{\omega})^{n-1} \exp(-2\nu k^2 \Delta t)\right] + \hat{\boldsymbol{f}}(k)\Delta t \tag{17}$$

where $\boldsymbol{u}$ are velocity vectors, a caret denotes Fourier transform, a superscript indicates the time step, and $\boldsymbol{f}$ is a small-wave-number forcing vector.

The computations are performed in a periodic $128^3$ cubic grid with domain side length $2\pi$ and viscosity $\nu = 1/3000$. The flow is initiated by a randomly perturbed velocity field with uniform probability distribution for wave numbers spanning the interval $1 \le k \le 64$. The

**Table 1 Quantities describing the isotropic turbulence simulation**

| Quantity | Value |
|---|---|
| $L$ | $2\pi$ |
| $\nu$ | 1/3000 |
| $u'$ | 0.057 |
| $\ell$ | 0.097 |
| $\lambda$ | 0.131 |
| $Re_\lambda$ | 22.3 |
| $\varepsilon$ | 0.00095 |
| $\eta$ | 0.014 |

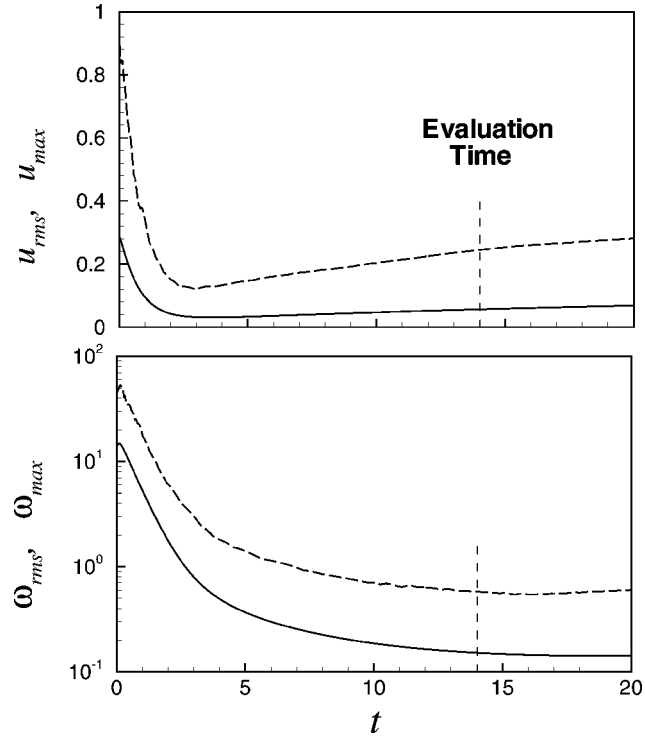


**Fig. 3 Time variation values of velocity and vorticity magnitude for a simulation of isotropic turbulence: – – –, maximum and ——, rms.**

turbulence is maintained by setting the forcing vector as

$$\hat{f} = \begin{cases} A\hat{\boldsymbol{u}}/\langle\hat{u}\rangle_< & \text{for} \quad k < k_{\text{crit}} \\ 0 & \text{for} \quad k > k_{\text{crit}} \end{cases} \tag{18}$$

where $\langle g\rangle_<$ denotes the average of a quantity $g$ for all wave numbers less than $k_{\text{crit}}$. The current computations are performed with $k_{\text{crit}} = 2$ and $A = 0.004$. The initial velocity field is made divergence-free by taking its Fourier transform and using the spectral form of the continuity equation. The time step for the computations is $\Delta t = 0.01$, and computations are continued until a time of $t = 20$ to let the turbulence develop. Various quantities describing the turbulence at the time chosen for evaluation ($t = 14$) are listed in Table 1, including the root-mean-square velocity magnitude $u'$, the average dissipation rate $\varepsilon$ [which can be written using energy conservation as $\varepsilon = -u'(\mathrm{d}u'/\mathrm{d}t)$], the integral length scale $\ell = 0.5u'^3/\varepsilon$, the Taylor microscale $\lambda = (15\nu/\varepsilon)^{1/2}u'$, the Kolmogorov length scale $\eta = (\nu^3/\varepsilon)^{1/4}$, and the microscale Reynolds number $Re_\lambda = u'\lambda/\nu$.

The time variation of the maximum and root-mean-square velocity and vorticity vectors are shown in Fig. 3. At the evaluation time, $t = 14$, these quantities are found nearly to approach an asymptotic value, indicating that the turbulence is reaching a statistically stationary state. The DNS data are filtered using an isotropic Gaussian convolution filter of form (1) with length scale $\Delta = 4\Delta x$, where $\Delta x = 0.05$ is the grid size for the DNS computation. The contours of the vorticity component $\omega_z$ in a cross section of the flow for both the DNS data and the filtered data are given in Fig. 4. The exact

**Table 2 Various correlations involving SGS force magnitude $g$, SGS torque magnitude $s$, filtered vorticity magnitude $\omega \equiv (\bar{\omega}_i\bar{\omega}_i)^{1/2}$, and enstrophy production rate $E \equiv \bar{\omega}_i\bar{S}_{ij}\bar{\omega}_j$ for exact data**

| Correlation | Isotropic turbulence | Turbulence near columnar vortex |
|---|---|---|
| $g$-$\omega$ | 0.822 | 0.912 |
| $s$-$\omega$ | 0.790 | 0.464 |
| $g$-$E$ | 0.364 | 0.094 |
| $s$-$E$ | 0.363 | 0.043 |

**Table 3 Correlations between exact data and predictions of the scale-similarity model for SGS force vector $g$ and SGS torque vector $s$**

| Correlation | Isotropic turbulence | Turbulence near columnar vortex |
|---|---|---|
| $\boldsymbol{g}_{\text{exact}}$-$\boldsymbol{g}_{\text{sim}}$ | 0.535 | 0.876 |
| $\boldsymbol{s}_{\text{exact}}$-$\boldsymbol{s}_{\text{sim}}$ | 0.366 | 0.434 |

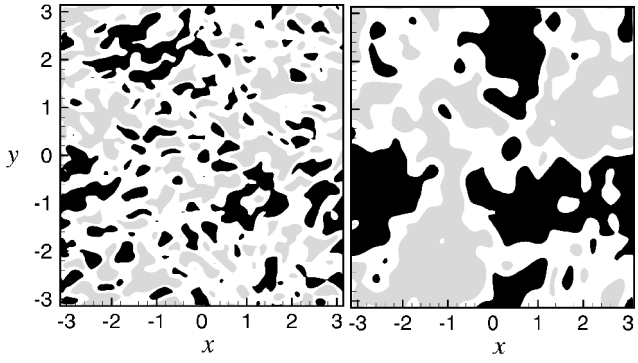


**Fig. 4 Contours of $\omega_z$ in a cross-section of the isotropic turbulence simulation for a) DNS data and b) filtered data: gray for $\omega_z > 0.04$ and black for $\omega_z < -0.04$.**

values (for the given filter) of the SGS force and torque are obtained by substituting the DNS data into Eq. (5) to obtain $\boldsymbol{g}$ and then taking its curl to get $\boldsymbol{s}$.

Correlations between the SGS force and torque and the vorticity magnitude and enstrophy production rate ($E \equiv \bar{\omega}_i\bar{S}_{ij}\bar{\omega}_j$) are listed in Table 2, where the correlation between any two scalar quantities $A$ and $B$ is defined by

$$C_{AB} \equiv \sum_i A_i B_i \Bigg/ \left[\left(\sum_j A_j^2\right)^{\frac{1}{2}}\left(\sum_k B_k^2\right)^{\frac{1}{2}}\right]$$

with the sum taken over the grid points. The inner product of two vectors is used instead in the numerator of this ratio for correlations between two vector-valued products. There are reasonably high correlations (roughly 80%) between the SGS force magnitude and the vorticity magnitude and between the SGS torque magnitude and the vorticity magnitude, whereas the correlation of these quantities with the enstrophy production rate is much lower (around 36%). This indicates that the SGS force and torque are strong in the vicinity of the strong vortex structures, but are not necessarily related to strong stretching rates. The correlation between the SGS force and torque magnitudes is also fairly high (82%), which indicates that regions of high SGS torque are likely to coincide with regions of high SGS force in isotropic turbulence.

Predictions comparing the scale-similarity model and exact data for the SGS force and torque magnitudes are given in Fig. 5. As shown in Table 3, both the predicted SGS force and torque vectors are found to have fairly low correlations with exact data (53 and 37%, respectively). On the other hand, the correlation for the predicted SGS force and torque magnitudes with exact data is fairly high (87 and 85%, respectively), which indicates that these quantities have large values in approximately the same regions of the flow in the

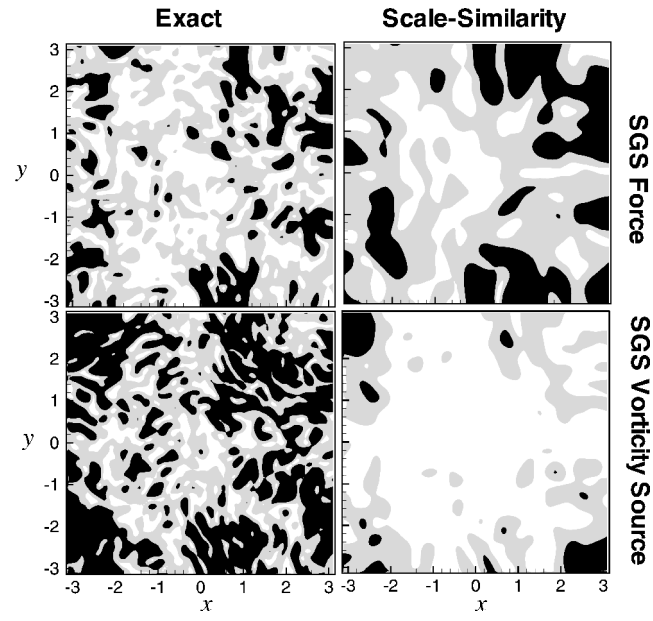


**Fig. 5 Comparison of exact data (left) and predictions of scale-similarity model (right) for magnitudes of SGS force (top) and SGS torque (bottom): SGS force magnitude, gray for $0.0025 < g < 0.005$ and black for $g > 0.005$ and SGS torque, gray for $0.001 < s < 0.002$ and black for $s > 0.002$.**

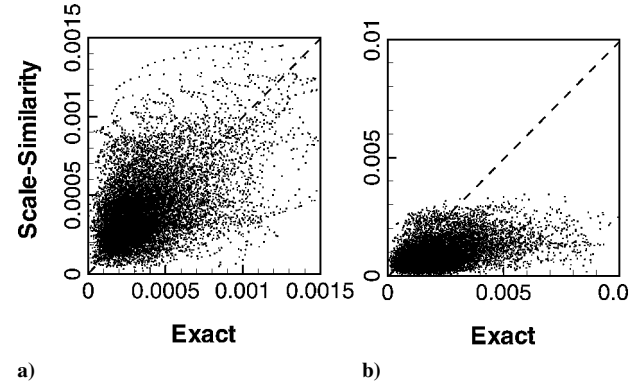


**Fig. 6 Scatter plots comparing exact data and scale-similarity model predictions for a) SGS force and b) SGS torque magnitude for isotropic turbulence.**

scale-similarity predictions and the exact data, but that the predicted and exact vectors have rather different orientation. Figure 5 shows that the scale-similarity predictions do not possess the small-scale structure present in the exact data. Although the predictions for maximum values of the SGS force agree reasonably well with the exact data, the predicted maximum values of the SGS torque are considerably lower than the exact data because the gradients of SGS force in the scale-similarity predictions are not as sharp. This tendency is clearly evident in the scatter plots of SGS force and torque shown in Fig. 6, in which the predicted values of SGS torque are observed to be generally significantly lower than the exact data. The poor ability of the scale-similarity model to predict SGS torque is related to the common observation that this model is not sufficiently dissipative, which leads to the necessity to add an eddy–viscosity term when this model is employed for LES computations.[16]

## V. Turbulence Near a Large-Scale Vortex

Most turbulent flows of engineering interest are not isotropic, but exhibit coherent eddy motions at an intermediate length scale. These coherent eddies dramatically alter the evolution of the surrounding smaller-scale turbulence. A DNS study illustrating this effect was reported by Melander and Hussain[17] for the problem of initially isotropic turbulence placed in the vicinity of a larger-scale columnar vortex. Their results demonstrate the wrapping of

the external turbulence about the columnar vortex and growth of turbulence length scales by merger of the nearly axisymmetric turbulent structures that result from wrapping. A similar computation was performed in the current study to examine the effect of coherent structures on the SGS torque within the surrounding turbulence.

The computation is performed using the numerical method described in the preceding section. The columnar vortex has Gaussian vorticity variation within its core with radial length scale $a = 0.6$, vortex Reynolds number $Re_V = \Gamma/\nu = 3000$ and maximum azimuthal velocity $u_v = \Gamma/2\pi a$. The turbulence is initialized by perturbing the columnar vortex flow by high-frequency velocity fluctuations with uniform probability distribution for wave numbers within the interval $30 \le k \le 34$ and with root-mean-square fluctuation velocity $u'$. Preliminary computations are performed with $64^3$ grid points to determine an appropriate value for the parameter $\beta = u'/u_v$, and the final computation is performed with $128^3$ grid points. The turbulence quickly decays away when $\beta$ is set too low, leaving just the columnar vortex. If $\beta$ is set too high, the columnar vortex is destroyed by the surrounding turbulence, leaving only decaying isotropic turbulence. We use an intermediate value $\beta = 1.12$ for which the vortex remains intact and the external turbulence becomes predominantly oriented in the azimuthal direction after a few rotations of the vortex. The time step is held fixed during the computations at $\Delta t = 0.01$, such that the Courant–Friedrichs–Lewy number $u_{\max}\Delta t/\Delta x$ is less than 0.05.

We interrogate the flow at a time $t = 50$, corresponding to a little over three and a half rotations of the large-scale vortex after the initial start. At this time, the maximum azimuthal velocity and axial vorticity of the large-scale vortex have decreased by about 10% of their initial values, to 0.145 and 0.78, respectively. The turbulence fluctuations have decreased in intensity by over an order of magnitude, such that the maximum velocity and vorticity fluctuations at the interrogation time are 0.034 and 0.41, respectively. The turbulence is more rapidly suppressed within the vortex core, due to the enhanced dampening induced by rotation,[18] and in the region far from the vortex. A region of active turbulence is found surrounding the vortex core, within which the vortex structures become aligned in the azimuthal direction and are stretched as they are entrained into the large-scale vortex core. This behavior is illustrated in the vorticity magnitude contour plots in the $x$–$y$ and $y$–$z$ cross-sectional planes shown in Fig. 7.

The DNS results are filtered using a Gaussian filter with length scale $\Delta = 4\Delta x$. The exact data for magnitude of SGS force and torque are shown in Fig. 8. In Fig. 8a, the regions of large SGS force magnitude are shown by gray and black shading and the regions of large axial vorticity $\omega_x$ are indicated by contour lines. The SGS force is observed to have the largest magnitude within the core of the large-scale vortex. However, similar to the case of a columnar vortex examined in Sec. III, the SGS force vector within the columnar vortex core is oriented mostly in the radial direction and varies mostly with the radial coordinate $r$, such that its curl is small. The SGS torque is found to have largest magnitude not within the vortex core, but in the region surrounding the core coinciding with the region of strong azimuthally oriented turbulence. In Fig. 8b, the regions of large SGS torque magnitude are indicated by gray and black shading, and solid and dashed contour lines indicate regions of strong positive and negative azimuthal vorticity $\omega_z$, respectively.

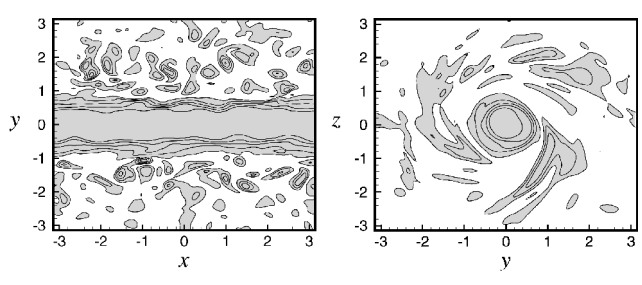


**Fig. 7 Contours of vorticity magnitude in the $x$–$y$ and $y$–$z$ cross-sectional planes for turbulence external to a columnar vortex; gray denotes regions with vorticity magnitude greater than 0.1.**

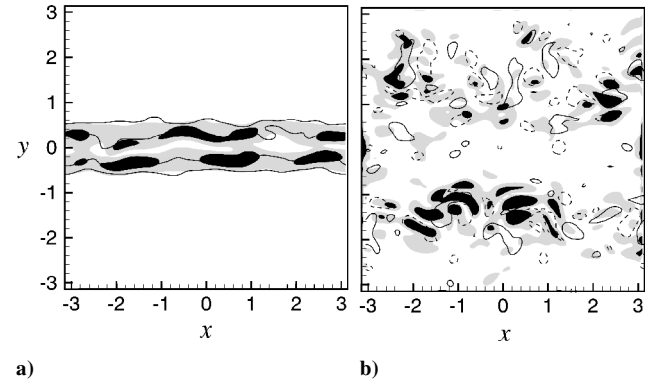


**Fig. 8 Comparison of a) SGS force, gray, $0.0025 < g < 0.005$; black, $g > 0.005$; and ——, axial vorticity contours with $\omega_x = 0.3$ and 0.5; and b) SGS torque magnitudes for turbulence external to a large-scale vortex, gray, $0.003 < s < 0.006$; black, $s > 0.006$; ——, $\omega_z = 0.7$ azimuthal vorticity contours; and – – –, $\omega_z = -0.1$ azimuthal vorticity contours.**

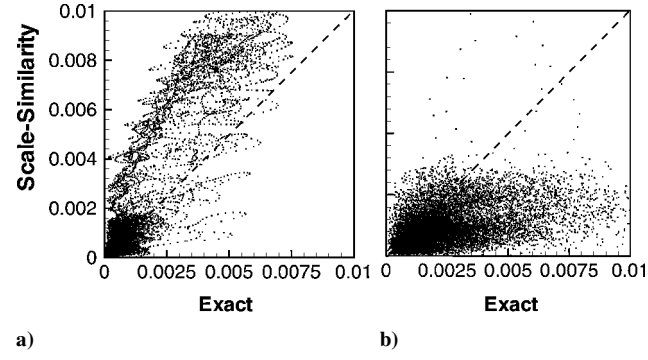


**Fig. 9 Turbulence near a large-scale vortex scatter plots comparing exact data and scale-similarity model predictions for a) SGS force and b) SGS torque magnitude.**

The observation that regions of strong SGS force are disjoint from regions of strong SGS torque is also apparent from inspection of the correlation values shown in Table 2. Although the SGS force has a high correlation with the vorticity magnitude (92%), the correlation between vorticity magnitude and SGS torque is fairly low (46%). The high correlation between the SGS force magnitude and the vorticity magnitude is mostly due to the radially oriented force that forms inside the large-scale columnar vortex, as shown in Fig. 8a. As explained in Sec. III, this force is not dynamically significant and, hence, does not give rise to a vorticity source. We recall that $\boldsymbol{s}$ vanishes for the purely columnar vortex flow considered in Sec. III, and correspondingly, the SGS torque is controlled by the azimuthal vorticity wrapping around the large-scale vortex.

Correlations between the scale-similarity predictions and exact data are given in Table 3. The predicted SGS force vector has a high correlation with the exact data (88%), whereas the predicted SGS torque vector has a fairly low correlation with exact data (43%). Scatter plots comparing magnitudes of predicted and exact SGS force and torque are given in Fig. 9. The predicted SGS force (Fig. 9a) is reasonably close to the exact data, with the predicted magnitude 20–30% larger than the exact magnitude. Similar overshoot in predicted force magnitude is found when the scale-similarity model is applied to the columnar vortex examined in Sec. III. On the other hand, the predicted SGS torque magnitude (Fig. 9b) is much too small. Detailed examination of the predictions and data indicate that, although the scale-similarity model reproduces with reasonable accuracy the dynamically insignificant radially oriented SGS force within the large-scale vortex core, it yields far too small values of the azimuthally oriented SGS torque.

## VI. Conclusions

The SGS torque is analyzed using a series of models of increasing complexity, including a single columnar vortex, isotropic

turbulence, and turbulence external to a columnar vortex, which mimic in different degrees the flow in the vicinity of a coherent vortex immersed in a high-Reynolds-number turbulent flow. The SGS torque is related to the dynamically significant parts of the SGS force and stress fields, but due to the presence of other parts of the SGS force and stress that do not influence the velocity field, the regions where the SGS torque is large do not always coincide to regions where the SGS force or stress are large.

The SGS torque vanishes for an isolated columnar vortex. If the vortex is immersed in an axial stretching flow, a SGS torque forms that acts to aid viscosity in diffusing the vorticity radially outward. By contrast, if the vortex is axially compressed the SGS torque acts to decrease the size of the vortex core.

For isotropic turbulence, the SGS force and vorticity fields are both found to be strong within regions of strong vorticity. The regions of large SGS force predicted by the scale-similarity model occurs in roughly the same locations as in the exact data, with roughly the same magnitude; however, the SGS force is much more diffuse and gradually varying in the model predictions than in the exact data. Consequently, the magnitude of the SGS torque predicted from the scale-similarity model is much too small. This observation is in fact the underlying reason for the common observation that the scale-similarity model does not have sufficient dissipation in a posteriori tests.

For turbulence external to a large-scale vortex, the SGS torque is found to be strongest not within the vortex core, but in the region of intense, azimuthally oriented vorticity structures that form a sheath around the large-scale vortex core. The SGS force, by contrast, is strongest within the core of the large-scale vortex, but is oriented in a radial direction and is nearly axisymmetric, to possess nearly zero curl. The SGS torque is, thus, found to originate from secondary features of the SGS force field. The scale-similarity model performs well in predicting the dynamically insignificant part of the SGS force, but yields values for SGS torque that are far lower than exact values.

## Acknowledgment

Computer time for this work was provided by a grant from the National Partnership for Advanced Computational Infrastructure, San Diego, California.

## References

[1]Meneveau, C., and Katz, J., "Conditional Subgrid Force and Dissipation in Locally Isotropic and Rapidly Strained Turbulence," *Physics of Fluids*, Vol. 11, No. 8, 1999, pp. 2317–2329.

[2]Domaradzki, J. A., Liu, W., and Brachet, M. E., "An Analysis of Subgrid-Scale Interactions in Numerically Simulated Isotropic Turbulence," *Physics of Fluids A*, Vol. 5, No. 7, 1993, pp. 1747–1759.

[3]Kerr, R. M., Domaradzki, J. A., and Barbier, G., "Small-Scale Properties of Nonlinear Interactions and Subgrid-Scale Energy Transfer in Isotropic Turbulence," *Physics of Fluids*, Vol. 8, No. 1, 1996, pp. 197–208.

[4]Bardina, J., Ferziger, J. H., and Reynolds, W. C., "Improved Subgrid-Scale Models for Large Eddy Simulation," AIAA Paper 80-1357, 1980.

[5]Rogallo, R., and Moin, P., "Numerical Simulation of Turbulent Flows," *Annual Review of Fluid Mechanics*, Vol. 16, 1984, pp. 99–137.

[6]Germano, M., Piomelli, U., Moin, P., and Cabot, W. H., "A Dynamic Subgrid-Scale Eddy Viscosity Model," *Physics of Fluids A*, Vol. 3, No. 7, 1991, pp. 1760–1765.

[7]Mansfield, J. R., Knio, O. M., and Meneveau, C., "A Dynamic LES Scheme for the Vorticity Transport Equation: Formulation and a priori Tests," *Journal of Computational Physics*, Vol. 145, 1998, pp. 693–730.

[8]Townsend, A. A., "On the Fine-Scale Spectrum of Turbulence," *Proceedings of the Royal Society London, Series A: Mathematical and Physical Sciences*, Vol. 208, 1951, pp. 534–542.

[9]Lundgren, T. S., "Strained Spiral Vortex Model for Turbulent Fine Structure," *Physics of Fluids*, Vol. 25, 1982, pp. 2193–2203.

[10]Pullin, D. I., Buntine, J. D., and Saffman, P. G., "On the Spectrum of a Stretched Spiral Vortex," *Physics of Fluids*, Vol. 6, No. 9, 1994, pp. 3010–3027.

[11]Saffman, P. G., and Pullin, D. I., "Anisotropy of the Lundgren-Townsend Model of Fine-Scale Turbulence," *Physics of Fluids*, Vol. 6, No. 2, 1994, pp. 802–807.

[12]Saffman, P. G., and Pullin, D. I., "Calculation of Velocity Structure Functions for Vortex Models of Isotropic Turbulence," *Physics of Fluids*, Vol. 8, No. 11, 1996, pp. 3072–3084.

[13]Pullin, D. I., and Saffman, P. G., "Reynolds Stresses and One-Dimensional Spectra for a Vortex Model of Homogeneous Anisotropic Turbulence," *Physics of Fluids*, Vol. 6, No. 5, 1994, pp. 1787–1796.

[14]Misra, A., and Pullin, D. I., "A Vortex-Based Subgrid Stress Model for Large-Eddy Simulation," *Physics of Fluids*, Vol. 9, No. 8, 1997, pp. 2443–2454.

[15]Vincent, A., and Meneguzzi, M., "The Spatial Structure and Statistical Properties of Homogeneous Turbulence," *Journal of Fluid Mechanics*, Vol. 225, 1991, pp. 1–20.

[16]Sarghini, F., Piomelli, U., and Balaras, E., "Scale-Similar Models for Large-Eddy Simulations," *Physics of Fluids*, Vol. 11, No. 6, 1999, pp. 1596–1607.

[17]Melander, M. V., and Hussain, F., "Coupling Between a Coherent Structure and Fine-Scale Turbulence," *Physical Review E*, Vol. 48, 1993, pp. 2669–2689.

[18]Bradshaw, P., "The Analogy Between Streamline Curvature and Buoyancy in Turbulent Shear Flow," *Journal of Fluid Mechanics*, Vol. 36, 1969, pp. 177–191.

H. M. Atassi
*Associate Editor*